Molecular motor crossing the frontier of classical to quantum tunneling motion

Samuel Stolz[a,b], Oliver Gröning[a,1], Jan Prinz[a,b], Harald Brune[b], and Roland Widmer[a]

[a]Empa, Swiss Federal Laboratories for Materials Science and Technology, 8600 Dübendorf, Switzerland; and [b]Institute of Condensed Matter Physics, École Polytechnique Fédérale de Lausanne, 1015 Lausanne, Switzerland

Edited by Ali Yazdani, Princeton University, Princeton, NJ, and approved May 7, 2020 (received for review October 24, 2019)

The reliability by which molecular motor proteins convert undirected energy input into directed motion or transport has inspired the design of innumerable artificial molecular motors. We have realized and investigated an artificial molecular motor applying scanning tunneling microscopy (STM), which consists of a single acetylene (C_2H_2) rotor anchored to a chiral atomic cluster provided by a PdGa(111) surface that acts as a stator. By breaking spatial inversion symmetry, the stator defines the unique sense of rotation. While thermally activated motion is nondirected, inelastic electron tunneling triggers rotations, where the degree of directionality depends on the magnitude of the STM bias voltage. Below 17 K and 30-mV bias voltage, a constant rotation frequency is observed which bears the fundamental characteristics of quantum tunneling. The concomitantly high directionality, exceeding 97%, implicates the combination of quantum and nonequilibrium processes in this regime, being the hallmark of macroscopic quantum tunneling. The acetylene on PdGa(111) motor therefore pushes molecular machines to their extreme limits, not just in terms of size, but also regarding structural precision, degree of directionality, and cross-over from classical motion to quantum tunneling. This ultrasmall motor thus opens the possibility to investigate *in operando* effects and origins of energy dissipation during tunneling events, and, ultimately, energy harvesting at the atomic scales.

molecular motor | scanning tunneling microscopy | surface science

In 1959, Richard Feynman envisioned downscaling of information storage and machines to atomic dimensions (1). Both visions were eventually realized: by writing information via positioning single atoms on a nickel surface in 1990 (2), and by devising the first artificial, light-driven molecular machine in 1999 (3). The latter has been inspired by molecular machines in biological systems (4, 5) and led to the design of countless artificial molecular machines (6–12). However, most synthetic molecular machines, although driven by quantum processes, exhibit classical kinetics (13, 14), whereas operation by quantum tunneling motion is largely elusive. Scanning tunneling microscopy (STM) provides an ideal platform for investigating the dynamics of atoms and molecules on surfaces (10–12, 15–22). However, few studies were aimed at achieving controlled, STM-tip position-independent, directional motion that requires breaking of inversion symmetry, which is commonly achieved by adsorbing chiral molecules on achiral surfaces (10–12, 15). We reverse this concept by using the surface of noncentrosymmetric PdGa crystals as chiral stator. This relaxes the geometric constraints on the rotor molecule, and allows directed motion even for simple and symmetric molecules such as C_2H_2.

The starting point of our study is the creation of a well-defined chiral surface from a noncentrosymmetric single crystal, namely the intermetallic compound palladium–gallium with 1:1 stoichiometry (PdGa) exhibiting bulk-terminated chiral surfaces (23). The chiral structure of some of these surfaces manifests itself in pronounced enantioselective adsorption properties (24). Here we choose the threefold symmetric $(\overline{111})$ surface of the PdGa A enantiomorph (23). Under appropriate ultrahigh vacuum preparation, it terminates by a layer containing three Pd atoms per trigonal surface unit cell ($a_0 = 6.95\mathring{A}$) forming an equilateral triangle of 3.01 Å side length (*SI Appendix*, Fig. S1 and ref. 25). The local inversion symmetry of this Pd trimer is lifted by coordination of the six second-layer Ga atoms and furthermore by three Pd atoms in the third layer (Fig. 1 *A* and *B*). In the following we will denote this termination as Pd_3.

On Pd_3, acetylene molecules adsorb on top of the Pd trimers (26). When imaged by STM at 5 K, they appear as dumbbells with lobe-to-lobe separation of about 3 Å in three symmetrically equivalent 120°-rotated orientations (Fig. 1 *E*–*G*) between which they switch quasiinstantaneously (Fig. 1 *C* and *D*). Acetylene molecules are firmly anchored to the trimer and usually dissociate before being dragged off the trimer by STM-tip manipulation.

We have followed the rotation events by recording tunneling current time series $I_T(t)$ at a fixed tip position (Fig. 1*H*), in analogy to the STM investigation of the rotation of chiral butyl–methyl–sulphide on Cu(111) (10). In the latter case, a weak (≤5%) asymmetry in the number of clockwise (CW) n_{CW} and counterclockwise (CCW) n_{CCW} rotations was reported and tentatively attributed to chiral STM tips, as no correlation of the directionality with the molecule's enantiomeric form was found. The $I_T(t)$ of Fig. 1*H*, recorded over $\Delta t = 100$ s, exhibits cyclic jump sequences between three levels ($\ldots R_A \rightarrow R_B \rightarrow B_C \rightarrow R_A \ldots$) with $n_{CCW} = 23$ jumps in the CCW direction and $n_{CW} = 0$ in CW, resulting in a frequency $f = \frac{n_{CCW}+n_{CW}}{\Delta t} = 0.23$ Hz and perfect directionality $dir = 100\% * \frac{n_{CCW}-n_{CW}}{n_{CCW}+n_{CW}} = 100\%$. Movie SV1 shows a

Significance

Conversion of undirected energy input into directed motion on molecular scales is the basis for controlled movements in living organisms. In this context, fundamental insights can be obtained by investigating artificial molecular machines under well-defined conditions. We devised the currently smallest, atomically precise molecular machine, whose rotor (C_2H_2) consists of just four atoms and whose functioning we have tracked employing scanning tunneling microscopy (STM). Unlike all other reported surface-anchored rotors, ours is characterized by an extremely high degree of directionality which is independent of STM-tip condition or position, therefore solely defined by the chiral support. Owing to its ultrasmall size, our rotor's operation crosses the well-established classical to an unanticipated quantum tunneling kinetic regime without loss in directionality.

Author contributions: S.S., O.G., J.P., and R.W. designed research; S.S., O.G., J.P., and R.W. performed research; S.S., O.G., J.P., and H.B. analyzed data; and S.S., O.G., H.B., and R.W. wrote the paper.

The authors declare no competing interest.

This article is a PNAS Direct Submission.

[1]To whom correspondence may be addressed. Email: oliver.groening@empa.ch.

This article contains supporting information online at https://www.pnas.org/lookup/suppl/doi:10.1073/pnas.1918654117/-/DCSupplemental.

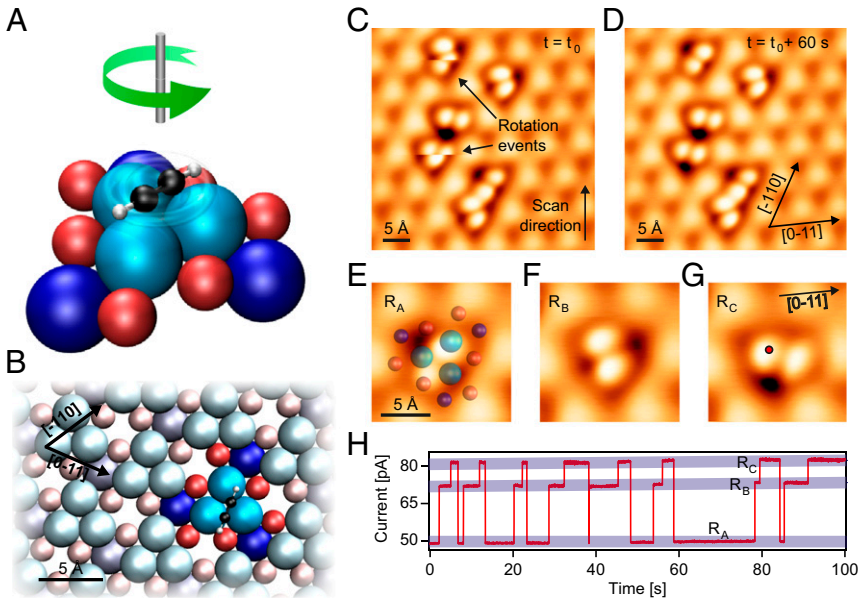

Fig. 1. Acetylene rotation on the PdGa:A($\overline{111}$)Pd_3 surface. (*A*) Sketch of the acetylene (C_2H_2) on Pd_3 motor. (*B*) Atomic structure of the PdGa:A($\overline{111}$)Pd_3 surfaces with the PdGa cluster acting as stator highlighted in saturated colors. The C_2H_2 rotor is depicted in one (R_a) of its three equivalent adsorption configurations R_a, R_b, R_c. In *A* and *B*, the top-layered Pd trimers ($z = 0$) are depicted in bright blue, the second-layer Ga trimers ($z = -0.85$ Å) in red, and the third-layered single Pd atoms ($z = -1.61$ Å) in dark blue. (*C*–*G*) Constant current STM images of C_2H_2 adsorbed on the Pd_3 surface ($T = 5$ K; $V_G = 10$ mV; $I_T = 50$ pA). In *C* two rotating molecules are pointed out, whereas in *D*, recorded 60 s after *C*, no molecular rotation is observed. (*E*–*G*) STM images of the same acetylene molecule in its three rotational configurations. In *E* the underlying PdGa stator structure is superposed. (*H*) Tunneling current time series $I_T(t)$ ($\Delta t = 100$ s; $V_G = 25$ mV; 1-ms time resolution) measured at the relative position to the C_2H_2 indicated by the red marker in *G*.

time-lapse series of STM images evidencing the prevailing CCW rotation of the motor.

Analyzing the parametric dependence of the rotation frequency (Fig. 2 *A*–*C* and *SI Appendix*, Fig. S2) shows that this molecular motor operates in two distinct regimes; the tunneling regime (TR) where its rotation frequency ν_T is independent of temperature $T < 15$ K, bias voltage $|V_G| < 30$ mV, and current $I_T < 200$ pA, and the classical regime (CR) where the frequency strongly depends on these parameters. Even though all experimental data presented in Fig. 1 have been recorded in the TR, we first discuss the CR where C_2H_2 rotations can be selectively powered by thermal or electrical excitations. We find the temperature dependence of the rotation frequency at low bias (Fig. 2*A*) to follow an Arrhenius characteristic (solid line in Fig. 2*A*) $\nu(T) = \nu_T + \nu_A \exp\left(-\frac{\Delta E_B}{k_B T}\right)$ **[1]**, with $\nu_T = 4.5$ Hz, $\nu_A = 10^{8.7\pm2.0}$Hz (attempt frequency), and $\Delta E_B = 27.5 \pm 7.1$ meV

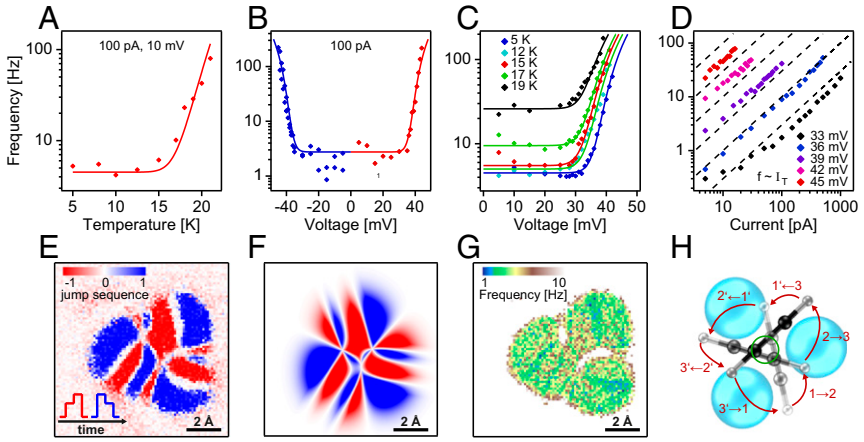

Fig. 2. Parametric dependence of the rotation frequency and jump sequence. (*A*) Rotation frequency dependence on temperature ($V_G = 10$ mV; $I_T = 100$ pA), *B* on bias voltage for both polarities ($T = 5$ K; $I_T = 100$ pA), *C* on bias voltage at various temperatures between 5 and 19 K; $I_T = 100$ pA), and *D* on tunneling current for different bias voltages between 33 and 45 mV at $T = 5$ K. In *A*–*D*, the markers represent experimental data, while the solid lines are derived from the kinetic model (*SI Appendix*). (*E*) Constant current jump-sequence map ($js = 3*\frac{n_{up}-n_{down}}{n_{up}+n_{down}} = sign(js)*|dir|$; $n_{up/down}$: number of jumps increasing/decreasing the tip height) generated from an 80 × 80 grid (1 × 1 nm^2) of individual tip-height time series $z_T(t)$, each recorded for 4 s (4,000 points; $V_G = 10$ mV; $I_T = 100$ pA). (*F*) Simulated jump-sequence map for a 100% CCW rotation based on the motion pattern shown in *H*. (*G*) Frequency map of the C_2H_2 rotation extracted from the same experimental $z_T(t)$ grid of *E*. (*H*) Our best estimation of the tumbling acetylene rotation on Pd_3 for a full 360° rotation in six 60° steps indicated by tracking the motion of one H atom (1→2→3→1′→2′→3′ with *n* and *n*′ denoting indistinguishable C_2H_2 configurations) with the green circle indicating the motion of acetylene's center of mass.

(energy barrier for rotation). Above 30 mV the frequency increases exponentially with V_G, independent of polarity (Fig. 2 *B* and *C*). Under the same conditions, but at constant bias voltage, the power-law dependence $\nu \propto I_T^n$ with $n \approx 1$ (Fig. 2*D*) identifies the electronically stimulated rotation as a single-electron process (27). As we will discuss later, the parametric dependence of the rotation frequency and directionality with T, V_G, and I_T is very well reproduced by a Langevin kinetic model (solid lines in Fig. 2 *B* and *C*).

Before we discuss the parametric dependence of the directionality, the influence of the STM tip, required for observing the motion, must be clarified. Particularly, we have to verify that breaking of the inversion symmetry due to the tip position (and possibly tip structure) in proximity to the motor does not prevail over the influence of the chiral substrate in determining the sense of rotation. To address this issue, we have measured 6,400 constant current tip-height time series $z_T(t)$ on a grid of 80×80 equidistant points covering 1×1 nm^2 in the vicinity of single acetylene molecules in the TR. Analysis of all these $z_T(t)$ series reveals an intricate, regular pattern with alternating, highly directional ascending (red) and descending (blue) jump sequences (Fig. 2*E*). This pattern fully corroborates a tip-position-independent, unidirectional rotation of the molecule, which becomes apparent by modeling and mapping the position-dependent jump sequence assuming a cyclic unidirectional CCW rotation of the molecule by 60° steps (*SI Appendix*, Figs. S4–S7). After optimizing molecule configuration and tip shape in the model, an excellent agreement of the simulated jump-sequence map (Fig. 2*F*) with the experiment is found. Hence, we conclude that, regardless of the tip position, the jump sequences always correspond to CCW rotations. Furthermore, as witnessed from Fig. 2*G*, there is no pronounced dependence of ν_T on the tip position, and all three rotational C_2H_2 configurations can be expected to be energetically equivalent, as derived from the residence time analysis in *SI Appendix*, Figs. S8–S10. The three rotational states only become energetically nondegenerate if the tip is brought very close to the substrate, such that it significantly alters the surface ratchet potential (*SI Appendix*, Fig. S3). Although we investigated hundreds of molecules with tens of different tip modifications, we never observed any systematic CW rotations in the TR or CR evidencing that solely the stator dictates the direction and directionality of the rotation. Evaluating 1,792 rotation events ($n_{CCW} = 1{,}771$ and $n_{CW} = 21$) in the TR, we determine a directionality $dir \geq 96.7\%$ with 2σ confidence. By matching the simulated jump-sequence map to the experiment we identify the C_2H_2 rotation to be best described as a tumbling rotor, whose center of mass moves on a circle with radius $r = 0.5 \pm 0.1$ Å and a moment of inertia $I_{C_2H_2} = 5.62 \times 10^{-46}$kgm^2 (Fig. 2*H*).

Having clarified the influence of the tip, we now turn to the discussion of the parametric dependencies of the directionality (Fig. 3 *A*–*D*). The temperature dependence shows a rapid drop in directionality once thermally activated rotations start to contribute significantly. The solid line in Fig. 3*A* assumes that ν_T exhibits 98% directionality, whereas the thermally activated jumps described by the Arrhenius equation **1** are purely random. These random thermal rotation events are expected because substrate, STM tip, and hence molecule are in thermal equilibrium and, accordingly, unidirectional rotation (which reduces entropy) is forbidden by the second law of thermodynamics. At $T = 5$ K a decrease of directionality is also observed for bias voltages V_G beyond ±35 meV (Fig. 3*B*). However, unlike thermal rotations, those induced by inelastic electron tunneling (IET) only become gradually nondirectional. This is clearly observed in the regime where thermally and IET induced rotations coexist. As displayed in Fig. 3*C*, the voltage-independent directionality of only 10% at $T = 19$ K and $|V_G| < 30$ mV, can be increased significantly at higher $|V_G|$ due to additional directed

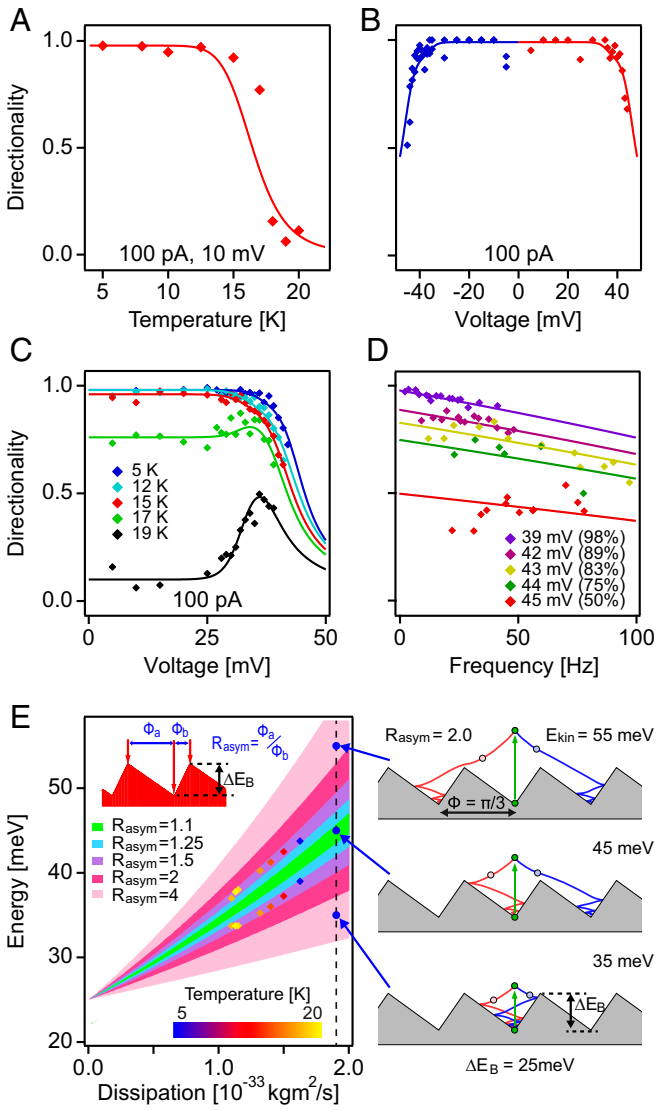

Fig. 3. Parametric dependence of the nanomotor's directionality. (*A*) Dependence of the directionality on temperature ($V_G = 10$ mV; $I_T = 100$ pA), (*B*) bias voltage for both polarities ($I_T = 100$ pA; $T = 5$ K), (*C*) bias voltage at various temperatures between 5 and 19 K ($I_T = 100$ pA), and (*D*) rotation frequency controlled via varying I_T for several V_G. In *A*–*D* the markers represent experimental data, while the solid lines in *A*–*C* are derived from the kinetic model (*SI Appendix*). The solid lines in *D* show simulated dependencies of constant directionality (given in brackets) with frequency considering finite time resolution of the experiment (*SI Appendix*). (*E*) Schematic representation of the Langevin rotation dynamics derived for ratchet potentials with $\Delta E_B = 25$ meV. (*Left*) The range of transferred kinetic energy E_{kin} for directed motion, i.e., $E_L < E_{kin} < E_R$, in dependence on energy dissipation is colored for several R_{asym}, as defined in the inset. The experimentally determined E_L and E_R are represented by two markers of the same color for several temperatures. (*Right*) The trajectories of the C_2H_2 60° rotation in a ratchet potential with $R_{asym} = 2.0$, $\lambda = 2{\times}10^{-33}\frac{\text{kgm}^2}{\text{s}}$ and $\Delta E_B = 25$ meV are displayed as a function of E_{kin}. From top to bottom: For $E_L < E_R < E_{kin}$ there is no unidirected motion, $E_L < E_{kin} < E_R$ results in directed motion by overcoming the steeper potential barrier, and $E_{kin} < E_L < E_R$ induces no rotation.

IET rotations. This increase is only effective in a narrow voltage window, above which the directionality rapidly decreases. By contrast, the I_T dependence of the directionality for a fixed voltage is weak (Fig. 3*D*), where the slight decrease with increasing current, i.e., frequency, is attributed to the detection of two rapidly successive CCW rotations as a single erroneous CW

one (solid lines in Fig. 3*D*). Hence we conclude that directionality stays above 95% for $|V_G| < 40$ mV even at high current.

The observation of directional motion triggered from a noncyclic, directionless, and position-independent energy input stemming from a single IET event, prompts us to apply a variant of the biased Brownian motion concept proposed by Astumian and Hänggi for modeling the underlying mechanism (28, 29). Our model of IET-induced rotation assumes a static, periodic, but asymmetric potential $U(\phi)$ ($\phi = [0,2\pi]$, with $\frac{\pi}{3}$ periodicity), with the asymmetry of the potential, R_{asym}, defined in Fig. 3*E*, *Inset* and *SI Appendix*, Fig. S11. A single IET event instantaneously excites the molecule from its ground state and its trajectory $\phi(t)$ is obtained from Langevin dynamics $I\ddot{\phi} = -\frac{\partial U(\phi)}{\partial \phi} - \lambda\dot{\phi}$, where I is the moment of inertia and λ the viscous dissipation coefficient (28, 29). Depending on R_{asym} and λ, two dissimilar minimum kinetic energies E_L and E_R are required to overcome the barrier to the left (i.e., CW) and to the right (i.e., CCW), respectively. These energies are the basis for describing frequency and directionality by the kinetic model (*SI Appendix*).

Matching this kinetic model to our experimental data in Figs. 2*C* and 3*C* allows determination of the temperature-dependent $E_L(T)$ and $E_R(T)$ which are represented by colored markers in Fig. 3*E*. From these values we deduce R_{asym} to be $1.25 < R_{asym} < 1.5$ assuming $\Delta E_B = 25$ meV. The reduction of the dissipation λ from about $1.6 \times 10^{-33} \frac{\text{kgm}^2}{\text{s}}$ at 5 K to around $1.1 \times 10^{-33} \frac{\text{kgm}^2}{\text{s}}$ at 20 K can be attributed to the less efficient coupling of the molecule to the substrate with increasing temperature.

Having successfully described the rich phenomenology of the over-the-barrier rotation processes in the CR, the unexpected, nearly perfect unidirectional rotation of C_2H_2 in the TR requires closer inspection. Tunneling, especially of hydrogen, is a well-established phenomenon in chemistry (30) and surface science (19), and plays a crucial role in numerous biological processes like enzyme-catalyzed reactions (31). The approximately exponential decrease of the tunneling rate with increasing mass, however, allows reasonably high tunneling rates of heavy atoms or molecules only for very small barrier heights and tunneling distances. Despite these restrictions, many tunneling transitions on surfaces involving heavy atoms like cobalt or small molecules have been reported (15, 20, 21, 32).

In this respect, the tunneling of formaldehyde (CH_2O) between two adsorption configurations on Cu(110) reported by Lin et al. is very close to the C_2H_2 rotation in terms of ΔE_B, moment of inertia, and rotation angle, and thus yields comparable frequencies ν_T (32). In both cases ν_T is critically tip-condition-dependent and varies between 0.01 and 0.1 Hz for CH_2O/Cu(110) and between 0.25 and 5 Hz for C_2H_2/Pd_3 surface. Thus, to evidence the strong isotopic dependence and corroborating quantum tunneling, we have paid attention that the ν_T for C_2H_2, fully (C_2D_2), and partially deuterated acetylene (C_2DH) are determined consecutively on the same sample with the same STM tip (*SI Appendix*, Fig. S15). Fig. 4*A* shows the resulting $I_T(t)$ sequences for C_2H_2, C_2DH, and C_2D_2 which reveal ν_T ratios (with respect to C_2H_2) of $1 : 0.56(11) : 0.24(5)$ (C_2H_2:C_2DH:C_2D_2), which we consistently observe with different tips (*SI Appendix*, Table ST3 and Fig. S16). This strong relative reduction of ν_T is contrasted by the comparatively small relative change of moment of inertia $1 : 1.08 : 1.2$ and thus indicative for quantum tunneling. Careful inspection of the $I_T(t)$ sequence of C_2DH with broken C_2 symmetry reveals that the rotation cycles through six rather than three current levels (Fig. 4*B*), which proves that a full acetylene rotation indeed requires six CCW 60° rotations. Comparison of the experimentally determined ν_T ratios to the corresponding Wentzel–Kramers–Brillouin (WKB) tunneling frequency (*SI Appendix*) shows an excellent match for a barrier height of $\Delta E_B = 25$ meV (Fig. 4*D*).

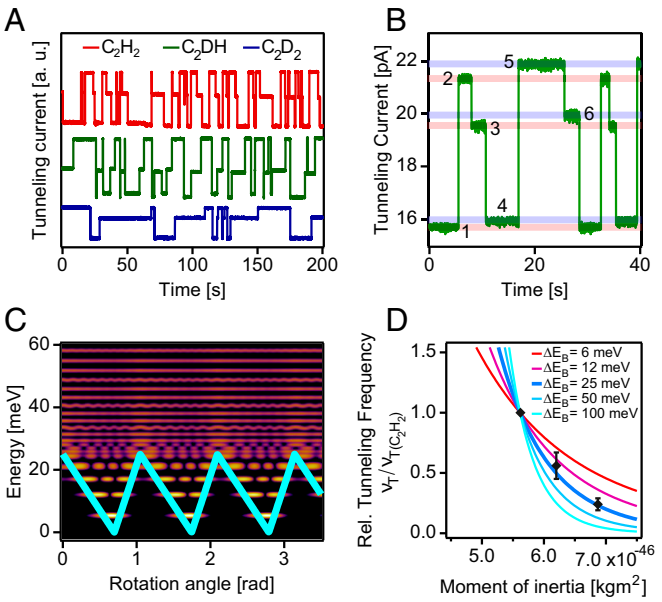

Fig. 4. Quantum tunneling rotation of acetylene. (*A*) $I_T(t)$ curves for C_2H_2, C_2DH, and C_2D_2, with a special focus on the six different current levels in an $I_T(t)$ curve of C_2DH in *B*. In *C* the ratchet potential is shown in turquoise, based on which the C_2H_2 quantum states, energy levels, and tunneling frequencies are determined. The color (black to yellow) represents the probability density of the quantum states. The dependence of ν_T in the WKB approximation with the moment of inertia, normalized to the ν_T at 5.62×10^{-46} kgm^2 (C_2H_2) is displayed as solid lines in *D* for several ΔE_B (*SI Appendix*). The black markers represent the experimental ν_T for C_2H_2, C_2DH, and C_2D_2, each normalized to the one of C_2H_2.

Quantum tunneling rotations concomitant with high directionality of 97.7% allow for an estimation of the entropy change of a single tunneling rotation from the experimental CCW and CW rotation probabilities, given by $\Delta S = -k_B \ln(p_{pCCW}/p_{CW}) \approx -k_B \ln(100/1) \approx -0.4 \frac{\text{meV}}{\text{K}}$. This implies that the directional rotation in the TR must be a nonequilibrium process with energy dissipation $\Delta Q > 2$ meV at 5 K and $\Delta Q > 6$ meV at 15 K per rotation. As these values of ΔQ are on the order of the energy difference of two frustrated rotation modes of C_2H_2 (e.g., $\hbar\omega_{10} - \hbar\omega_{00} = 6.8$ meV; Fig. 4*C* and *SI Appendix*, Fig. S14 and Table ST2), one might assume that the required nonequilibrium tunneling proceeds via an excitation from the ground state to a bound rotational mode as proposed by Nacci et al. (21). We estimate a maximum power dissipation of 100 meV/s per motor, assuming 10-Hz tunneling frequency as upper bound. On the other hand, the STM required for monitoring the rotation, locally dissipates at least 3×10^6 meV/s even at the lowest settings of 1-pA tunneling current and 0.5-mV bias. We still observe the constant rotation frequency with persisting high directionality at such extreme settings. Therefore, the STM tip is presumably critical in driving the system out of equilibrium also in the regime of tunneling motion.

In conclusion, the highly directional tumbling rotation of C_2H_2 on the chiral PdGa{111}Pd_3 surfaces exhibits a rich phenomenology, most prominently characterized by an unprecedentedly high directionality and small motor size. Its rotor (C_2H_2) and stator (Pd_3-Ga_6-Pd_3 cluster) shown in Fig. 1*A* comprise just 16 atoms to form a unidirectional six-state cyclic molecular motor (Fig. 4*B*) through all of which it cycles ceaselessly, powered exclusively by single electrons. This contrasts reported motors driven by light or chemical reactions, since for the former concerted thermal and light-driven activation is required. The latter usually requires a cycling of the chemical environment to complete

one cycle. In the classical regime, we could establish a Langevin kinetic model of the motion describing frequency and directionality with temperature, STM bias voltage, and tunneling current. The model provides robust values for the rotational potential asymmetry R_{asym} and the temperature dependence of the viscous dissipation coefficient $\lambda(T)$ relating the operation of this molecular machine to atomic friction. The negative entropy change associated with the high rotation directionality, also observed in the tunneling regime, challenges the understanding of this simple cyclic machine in terms of dissipative quantum tunneling dynamics (33). In the future, it might be possible to convert energy via forced excitations, e.g., optical, or by IET, into directional motion and thus investigating energy harvesting at the smallest possible length scale.

Materials and Methods

All experiments were performed under ultrahigh vacuum conditions with a base pressure below 5×10^{-11} mbar using an Omicron low-temperature STM operated at 5 K. The measurements were performed with different tips including 80:20 Pt/Ir tip, Tungsten STM, and Tungsten Q+ Sensor tips. We have found no systematic difference in the experimental results obtained with different tips. The PdGa crystal surface was prepared by repeated sputter and annealing cycles (sputtering: Ar^+, 1 keV; annealing: 20 min at 870 K).

Before dosing C_2H_2, which was purchased from PanGas with a purity of 99.6%, the gas line was precleaned by purging with the gas or by freeze–thaw cycling (77 K). In case of C_2D_2, purchased from CDN isotopes with 99% purity (C_2DH being the impurity), no precleaning was performed, because the gas was bottled with atmospheric pressure. Both gases were dosed by chamber backfilling through a leak valve at a pressure of 2×10^{-9} mbar. By removing the sample from the STM stage at 5 K exposing it to the acetylene outside the cryostat for a short time (generally 10–20 s) the most effective exposure conditions were achieved.

Data and Materials Availability. The datasets generated and/or analyzed during the current study are available from the corresponding author on reasonable request.

The simulations used in the current study have been performed using a custom-made code on the Wave Metrics IGOR Pro platform. Details of this code can be obtained from the corresponding author upon reasonable request.

ACKNOWLEDGMENTS. We thank R. Fasel for carefully reviewing the manuscript and Carlo Pignedoli for performing DFT calculations of the rotor. We acknowledge funding from the Swiss National Science Foundation under SNSF Project 159690.

1. R. P. Feynman, There's plenty of room at the bottom. *Eng. Sci.* **23**, 22–36 (1960).
2. D. M. Eigler, E. K. Schweizer, Positioning single atoms with a scanning tunnelling microscope. *Nature* **344**, 524–525 (1990).
3. N. Koumura, R. W. J. Zijlstra, R. A. van Delden, N. Harada, B. L. Feringa, Light-driven monodirectional molecular rotor. *Nature* **401**, 152–155 (1999).
4. K. Svoboda, C. F. Schmidt, B. J. Schnapp, S. M. Block, Direct observation of kinesin stepping by optical trapping interferometry. *Nature* **365**, 721–727 (1993).
5. M. Schliwa, G. Woehlke, Molecular motors. *Nature* **422**, 759–765 (2003).
6. V. Balzani *et al*., Autonomous artificial nanomotor powered by sunlight. *Proc. Natl. Acad. Sci. U.S.A.* **103**, 1178–1183 (2006).
7. D. Roke, S. J. Wezenberg, B. L. Feringa, Molecular rotary motors: Unidirectional motion around double bonds. *Proc. Natl. Acad. Sci. U.S.A.* **115**, 9423–9431 (2018).
8. J. V. Hernández, E. R. Kay, D. A. Leigh, A reversible synthetic rotary molecular motor. *Science* **306**, 1532–1537 (2004).
9. S. Erbas-Cakmak *et al*., Rotary and linear molecular motors driven by pulses of a chemical fuel. *Science* **358**, 340–343 (2017).
10. H. L. Tierney *et al*., Experimental demonstration of a single-molecule electric motor. *Nat. Nanotechnol.* **6**, 625–629 (2011).
11. T. Kudernac *et al*., Electrically driven directional motion of a four-wheeled molecule on a metal surface. *Nature* **479**, 208–211 (2011).
12. Y. Zhang *et al*., A chiral molecular propeller designed for unidirectional rotations on a surface. *Nat. Commun.* **10**, 3742 (2019).
13. S. Kassern *et al*., Artificial molecular motors. *Chem. Soc. Rev.* **46**, 2592–2621 (2017).
14. C. Pezzato, C. Cheng, J. F. Stoddart, R. D. Astumian, Mastering the non-equilibrium assembly and operation of molecular machines. *Chem. Soc. Rev.* **46**, 5491–5507 (2017).
15. A. J. Heinrich, C. P. Lutz, J. A. Gupta, D. M. Eigler, Molecule cascades. *Science* **298**, 1381–1387 (2002).
16. U. G. Perera *et al*., Controlled clockwise and anticlockwise rotational switching of a molecular motor. *Nat. Nanotechnol.* **8**, 46–51 (2013).
17. G. J. Simpson, V. García-López, A. Daniel Boese, J. M. Tour, L. Grill, How to control single-molecule rotation. *Nat. Commun.* **10**, 4631 (2019).
18. B. C. Stipe, M. A. Rezaei, W. Ho, Coupling of vibrational excitation to the rotational motion of a single adsorbed molecule. *Phys. Rev. Lett.* **81**, 1263–1266 (1998).
19. L. J. Lauhon, W. Ho, Direct observation of the quantum tunneling of single hydrogen atoms with a scanning tunneling microscope. *Phys. Rev. Lett.* **85**, 4566–4569 (2000).
20. J. A. Stroscio, R. J. Celotta, Controlling the dynamics of a single atom in lateral atom manipulation. *Science* **306**, 242–247 (2004).
21. C. Nacci *et al*., Current versus temperature-induced switching in a single-molecule tunnel junction: 1,5 cyclooctadiene on Si(001). *Nano Lett.* **9**, 2996–3000 (2009).
22. K. Sun *et al*., Supramolecular motors on graphite surface stabilized by charge states and hydrogen bonds. *ACS Nano* **11**, 10236–10242 (2017).
23. D. Rosenthal *et al*., Surface investigation of intermetallic PdGa($\overline{111}$). *Langmuir* **28**, 6848–6856 (2012).
24. J. Prinz, O. Gröning, H. Brune, R. Widmer, Highly enantioselective adsorption of small prochiral molecules on a chiral intermetallic compound. *Angew. Chem. Int. Ed. Engl.* **54**, 3902–3906 (2015).
25. J. Prinz *et al*., Isolated Pd sites on the intermetallic PdGa(111) and PdGa(-1-1-1) model catalyst surfaces. *Angew. Chem.* **124**, 9473–9477 (2012).
26. J. Prinz *et al*., Adsorption of small hydrocarbons on the three-fold PdGa surfaces: The road to selective hydrogenation. *J. Am. Chem. Soc.* **136**, 11792–11798 (2014).
27. S. Gao, M. Persson, B. I. Lundqvist, Theory of atom transfer with a scanning tunneling microscope. *Phys. Rev. B* **55**, 4825–4836 (1997).
28. R. D. Astumian, S. Mukherjee, A. Warshel, The physics and physical chemistry of molecular machines. *ChemPhysChem* **17**, 1719–1741 (2016).
29. P. Hänggi, F. Marchesoni, Artificial Brownian motors: Controlling transport on the nanoscale. *Rev. Mod. Phys.* **81**, 387–442 (2009).
30. P. R. Schreiner, Tunneling control of chemical reactions: The third reactivity paradigm. *J. Am. Chem. Soc.* **139**, 15276–15283 (2017).
31. J. P. Klinman, A. Kohen, Hydrogen tunneling links protein dynamics to enzyme catalysis. *Annu. Rev. Biochem.* **82**, 471–496 (2013).
32. C. Lin, E. Durant, M. Persson, M. Rossi, T. Kumagai, Real-space observation of quantum tunneling by a carbon atom: Flipping reaction of formaldehyde on Cu(110). *J. Phys. Chem. Lett.* **10**, 645–649 (2019).
33. A. O. Caldeira, A. J. Leggett, Influence of dissipation on quantum tunneling in macroscopic systems. *Phys. Rev. Lett.* **46**, 211–214 (1981).